Theoretical investigation of the band alignment of graphene on a polar SrTiO_{3} (111) surface

Donghan Shin and Alexander A. Demkov

Phys. Rev. B **97**, 075423 — Published 20 February 2018

DOI: 10.1103/PhysRevB.97.075423

Theoretical investigation of the band alignment of graphene on a polar $SrTiO_3$ (111) surface

Donghan Shin and Alexander A. Demkov*

Department of Physics, The University of Texas at Austin, Austin, TX 78712, USA

Abstract

Doping graphene layers presents a difficult practical and fundamental problem. We consider theoretically, the possibility of electrostatic doping of graphene by the intrinsic field of a polar substrate. By way of example, we perform density functional theory calculations for a graphene sheet placed on the (111)-oriented perovskite $SrTiO_3$ surface. We find that the Fermi surface moves well below the Dirac point of graphene, resulting simultaneously in a fast conducting channel in graphene, and a slow (large-effective-mass) channel at the oxide surface. Additionally, electrostatic gating may open a way to explore peculiar states that, through the "no-crossing", represent a hybrid carrier that exists simultaneously in both materials.

I. Introduction

Graphene is a two-dimensional single-atom-thick carbon layer with a honeycomb lattice structure. It is a zero-gap-semiconductor that has a linear energy dispersion near the Fermi level [1,2]. After the initial report of exfoliating graphene [3], the material has been extensively studied and has impacted significantly the physics of low-dimensional systems. Since pristine graphene has very high electron mobility [4], it is expected to have potential applications in electronics. However, as pristine graphene has no band gap, the ability to control the carrier density by doping or gating is of key importance. Substitutional chemical doping has been achieved using nitrogen (N) and boron (B) to produce n- and p-type graphene, respectively, as the atomic radii of carbon, N, and B are comparable [5-9]. However, chemically doped samples are highly defective resulting in low mobility, and growing N- and B-doped graphene is difficult [10]. There are several reports on gated graphene with silica (SiO_2) used as the supporting substrate [11-27]. This approach, however, encountered several critical problems, such as the low dielectric constant of SiO_2. As a result, most current research on gated graphene is focused on replacing SiO_2 with boron nitride [28] or non-volatile polymers [29,30]. However, there are difficulties in exfoliating and identifying graphene on these substrates [31]. There are several reports of graphene integrated with complex oxides demonstrating the feasibility of this approach. Hong et al. and Zheng et al. have reported a graphene/ferroelectric $Pb(Zr,Ti)O_3$ hybrid device [30,32]. Jin et al. proposed a design of ferroelectric-gated graphene-based devices using $LiNbO_3$ [33]. Gogoi et al. investigated optical properties of graphene on (100)-oriented $SrTiO_3$ [34]. In addition, Khomyakov et al. have reported a theoretical study of doping of graphene on metal substrates due to charge transfer [35] that suggested an interesting alternative to substitutional doping and possibly a way to preserve graphene's mobility.

In 2004, another intriguing physical phenomenon was reported at the interface between a polar and non-polar oxides. Ohtomo and Hwang demonstrated the presence of a high mobility two-dimensional electron gas (2DEG) at the interface of a (001)-oriented $SrTiO_3/LaAlO_3$ (STO/LAO) perovskite heterostructure [36]. The origin of conductivity is still under debate but has been explained in part by electrostatic doping due to the "polar catastrophe" [37-39]. Viewed along the (001) axis, LAO consists of alternating charged atomic planes and as a result, the electrostatic potential across the film diverges with LAO thickness. In semiconductors, such 'polar catastrophe' causes atomic reconstruction [37] and a similar mechanism operates in stand-alone LAO films [40]. However, at the oxide interface electronic reconstruction can occur instead, which can result in extremely high doping levels [37,38]. Indeed, Huang et al. have reported a theoretical study of field doping of graphene using a SiC substrate [41] and Chen et al. have investigated experimentally hole doping of epitaxial graphene using thin films of MoO_3 [42].

Here we use first-principles theory to explore the effect of polar STO substrate on the electronic structure of single layer graphene. We propose that placing a layer of graphene on a (111)-oriented $SrTiO_3$ with its highly charged alternating layers of SrO_3^{4-} and Ti^{4+}, may be a promising way to achieve high levels of doping. Unlike SiO_2, STO also has a rather large dielectric constant, which can provide reduced gate leakage, improved gate capacitance, and better gate modulation [43]. The rest of the paper is organized as follows. We briefly describe the theoretical methodology in Sec. II. In Sec. III, we discuss the band alignment at the graphene/STO interface, electrostatic doping of graphene, and the transport properties of graphene on the (111) STO support.

II. Theoretical methodology

All calculations are done within the density functional theory (DFT) as implemented in the Vienna *ab initio* simulation package (VASP) code [44]. We employ the generalized-gradient approximation (GGA) to the exchange correlation energy functional. We use projector-augmented-wave pseudopotentials [45] to describe Sr, Ti, O, and C, and a cutoff energy of 450 eV is used. We consider valence electron configurations $4s^24p^65s^2$ for Sr, $3p^64s^23d^2$ for Ti, $2s^22p^4$ for O, and $2s^22p^2$ for C. Each self-consistent electronic calculation is converged to within 10^{-5} eV per cell, and the ionic relaxation is performed until the forces are less than 0.01 eV/Å. To account for the dipolar interaction between the graphene layer and STO substrate, the van der Waals correction is included using the DFT-D2 method [46]. We obtain a lattice constant of 3.95 Å for bulk STO in good agreement with the experimental value of 3.91 Å. For bulk graphene we obtain a lattice constant of 2.47 Å, which agrees well with the experimental value of 2.46 Å. We calculate a Fermi velocity of 0.94×10^6 m/s for the bulk graphene, in excellent agreement with the previously reported LDA-based value of 0.95×10^6 m/s [47]. We use a nine-layer-thick (111)-oriented SrO_3-terminated symmetric vacuum STO slab with a 3×3 surface cell and a 7×7 graphene layer as shown in Fig. 1. We put graphene sheets on both the top and

bottom SrO_3-terminated surface to match periodic boundary conditions. When considering a 3 × 3 STO (111) surface and a 7 × 7 graphene sheet, the in-plane lattice constant of the cell is fixed to $3 \times \sqrt{2}\, a_{STO}$ =16.74 Å, resulting in a lattice mismatch of only 3.3 % for GGA-optimized materials. We have considered the surface reconstruction of STO (111), but did not include this effect here as its effect on the electronic structures is relatively small. The optimized distance *d* between the graphene layer and STO substrate is found to be 3.0 Å, no further relaxation was included. The symmetric SrO_3-termination is used for both top and bottom surfaces and graphene layers are placed on both sides of the slab. We use 9 Å of vacuum to prevent the interaction between periodic images of the system. For bulk and supercell structures, we use 8 × 8 × 8 and 6 × 6 × 1 k-point meshes, respectively.

III. Results and Discussion

A. Band alignment

A conduction-band offset can usually be estimated using the metal-induced gap states (MIGS) model [48]. In this model, when a metal is brought in contact with a semiconductor, the resulting conduction-band offset (Δ) is given by [49,50]:

$$\Delta = S(\Phi_M - \Phi_S) + (\Phi_S - \chi), \qquad (1)$$

where Φ_M is the work function of the metal, Φ_S is the charge neutrality level (CNL) of the semiconductor with respect to vacuum level, and χ is the electron affinity. S is the Schottky pinning parameter representing the screening by the interfacial states. If $S = 1$, Δ is given simply by the difference between the work function and the electron affinity, which represents the Schottky limit [51]. When $S = 0$, Δ is given by the difference between the CNL and the affinity, which is the Bardeen limit [52]. It suggests that the barrier height is determined by the intrinsic, complex oxide band structure and is independent of the metal [50]. In Fig. 2, we schematically show the band alignment in the Schottky limit using experimental values for the affinity and band gap of STO, and the work function of graphene [49,50,53-56]. Interestingly, Δ is expected to be 0.7 eV both in the Schottky and Bardeen limits, as the work function of graphene value coincides with the CNL of STO [54,56]. However, we believe that the often quoted CNL position of STO in the upper half of the band gap is not intrinsic, but is due to the well-documented oxygen deficiency in STO [57-59]. Using the CNL value estimated theoretically from the complex band structure of STO [50], Δ is expected to be 1.9 – 2.5 eV. Note that in this case, the CNL is well below the Fermi level of graphene, making charge transfer into the oxide evanescent states possible, at least in principle.

One can also try to predict the band alignment using the DFT-based reference potential and layer-projected density of states methods to determine the position of the STO and graphene spectra with respect to the vacuum level. Placing a graphene sheet in a large simulation box, we find that the Fermi level is 4.23 eV below vacuum, in fair agreement with the experimental work function value of 4.6 eV [55]. We then consider a symmetric, twenty seven-layer-thick, (111)-

oriented STO slab. The position of the valence band maximum (VBM) and conduction band minimum (CBM) in the bulk region can be found using the reference potential method [48,60]. The plane averaged electrostatic potential for a half of the simulation cell is shown in Figure 3, along with the density of states projected on every atomic plane. The band gap of 1.78 eV is found in the bulk region, underestimated compared with the experimental value of 3.2 eV [53]. The GGA band gap is close to the LDA result (1.8 eV), but is smaller than 3.2 eV obtained with the hybrid-functional [61]. The Fermi level is 5.83 eV below the vacuum and cuts across the top of the valence band of the surface layer, creating a hole pocket. The bulk VBM and CBM are 6.0 and 4.19 eV below the vacuum level, respectively. At the surface, the CBM and VBM are slightly higher in energy due to band bending. At the surface, the electron affinity (χ_S) is close to 4.0 eV, but is 4.16 eV 15 Å below the surface. The graphene bands near the Dirac point are schematically shown in the right part of the figure; on a technical side, we would like to point out that in the Schottky limit, the Fermi level of graphene lies in the gap of STO within this theory, again pointing to a possible charge transfer upon contact. The peculiar feature of this system is that the density of states at the Fermi level of the metal (graphene) is significantly lower (actually zero at the Dirac point itself) than that at the CNL of the insulator (STO), making the very assumptions of the MIGS model suspect. Thus a real calculation, with both materials in contact is necessary.

B. Substrate Doping of Graphene

In Fig. 4 we show the layer-by-layer atom-projected density of states (pDOS) when the graphene sheets placed on the symmetrically terminated (111) STO surface. The top and bottom surfaces of the STO slab are SrO_3-terminated (see Fig. 1), so the electric field is suppressed by the symmetry. Only half of the simulation cell is shown because the other half is just a mirror image. As can be clearly seen in the figure, the top SrO_3 surface is p-type. Most importantly, the Fermi level (0.72 eV) is well below the Dirac point of graphene, indicating graphene doping. The mechanism is charge transfer from the lower Dirac cone to the unoccupied surface states of the oxide substrate (the hole pocket shown in Fig. 3). For comparison, we have also considered graphene sheets placed on a stoichiometric (111) STO slab to see if there is an effect on the STO surface electronic structure. To maintain the overall periodicity in the stacking direction, a two-slab cell with mirror-symmetry was used (not shown). In this case, each slab has both SrO_3- and Ti-terminated surfaces, so the electric field is present across the slab. We compare the pDOS of the symmetric slab (no internal field) with that of the SrO_3 surface of the stoichiometric slab (with a field across) and find that the pDOS of the top five layers of each slab is very similar. A hole pocket can be seen at the SrO_3-terminated surface in both cases (the Ti-terminated surface of the stoichiometric slab is n-type). In these p-type surfaces, the oxide states around the Fermi level are mainly derived from the oxygen p-state. The mechanisms are of course somewhat different, but the robust feature is the electron acceptor nature of the SrO_3-terminated (111) surface.

In Fig. 5 we show the near-edge electronic structure and corresponding charge distribution of the system. In Fig. 5(a) we can see a linear energy dispersion and the crossing point, corresponding to the Dirac point of graphene, 0.72 eV above the Fermi level around the high symmetry point (1/3, 1/3, 0). The band structure of a pure graphene 7×7 supercell is superimposed (a dashed line) for clarity. One can clearly see the p-type doping of graphene. However, the Fermi surface is actually distributed between the two materials. The flat, dispersionless bands seen around the Fermi level are derived from the oxygen-dominated valence states of the STO substrate. The near-edge electronic structure is better understood when considering the probability distribution and charge density for empty and occupied states, respectively, shown in Fig. 5(b) and (c). The empty states within the energy window near the linear band crossing (the Dirac point), clearly show a π-bonding-like probability distribution localized on the graphene sheet. This is consistent with the electronic structure of pristine graphene and stems from the π-bonding of carbon atoms [62]. The charge density corresponding to the energy window near the Fermi level (Fig. 5(c)) shows a charge distribution of occupied states spread over both the graphene sheet and oxide surface. The charge density in STO is localized around the oxygen atoms in the substrate, indicating they are derived from the STO valence bands. The charge distribution in graphene is mainly composed of π-like carbon-based orbitals. This result suggests the formation of two conducting channels, one in graphene and one across the STO surface.

C. Hybrid Carriers

To explore further the electronic interaction between the graphene layers and the STO (111) slab, in Fig. 6 we show the electronic structure near the Fermi level in greater detail and identify the contribution of graphene to the band structure, and the corresponding probability density of the system. If we trace the graphene-derived linear band away from the crossing at (1/3, 1/3, 0) towards the Γ point at (0, 0, 0), it intersects five STO-derived bands approximately 0.2 eV above the Fermi level. An avoided crossing is seen at 0.11 eV above the Fermi level, where the graphene band opens a gap of 0.05 eV at (0.184, 0.184, 0). Under a proper bias this would render graphene a small-band gap semiconductor (the gap is twice the value of kT at room temperature). This mini band-gap opening stems from the interaction between graphene and STO. In the mini-gap region, linear bands (blue dots in Fig. 6(a)) derived from graphene and the flat bands (red dots in Fig. 6(a)) composed of the STO surface states repel. To illustrate the effect, we use a simple two-band model. To build the Hamiltonian, we take two states, one from graphene and one from STO: $|1\rangle$ = graphene state, $|2\rangle$ = STO surface state. In this basis we construct a tight-binding model Hamiltonian (the energy is referenced to the Fermi level),

$$\begin{pmatrix} E_1 & \Delta \\ \Delta^* & E_2 \end{pmatrix}, \tag{2}$$

where $E_1 = \hbar v_F k$, v_F is the Fermi velocity, $E_2 = 0.075$ eV, and Δ is the coupling strength between the two states. The Fermi velocity is calculated using the slope of the linear dispersion, obtaining 0.81×10^6 m/s. This Hamiltonian gives an energy dispersion near the gap, $E_{\pm}(k) =$

$\frac{1}{2}(E_1+E_2)\pm\sqrt{\left(\frac{E_1-E_2}{2}\right)^2+|\Delta|^2}$. Our GGA calculation shows a splitting of about 0.05 eV, which means that the coupling strength is approximately 0.025 eV. The two-band model is in good agreement with the GGA calculation as shown in Fig. 6(a). Interestingly, there are upper and lower branches of a graphene-derived linear band and dispersionless STO bands. However, between these two distinct parts, there are mixed states that are neither purely graphene-like nor purely STO-like. The probability distributions corresponding to each of these two distinct states are shown in Fig. 6(b) and (c). The probability density corresponding to the STO bands (Fig. 6(b)) shows that the dispersionless STO bands originate mainly from the oxygen atoms in the STO surface layer. However, when we calculate the probability density corresponding to the no-crossing region (Fig. 6(c)), we can see the distribution around both the graphene layer and the STO surface layer. We interpret these states as hybrid carriers having mixed-character introduced by the coupling between graphene and STO. Though these mixed states are not at the Fermi level, application of a small gate potential can easily shift conduction into this interesting regime.

IV. Conclusions

In summary, our theoretical calculations suggest that placing graphene on STO (111) results in p-type doping of graphene, and causes the formation of two conducting channels near the Fermi level: A fast channel in graphene and a slow one (due to a large effective mass) in the oxide surface layer. In addition, as the graphene linear band intersects the flat bands of STO, the interaction between the two bands opens a mini-gap due to the avoided crossing. The calculations predict mixed-character states around the mini-gap which can be accessed by electrostatic gating. The observed p-type doping is a consequence of the SrO_3 termination of STO, but the substrate can be Ti-terminated as well. In this case, graphene will become n-type doped. This creates the tantalizing possibility of building a p-n junction by laying a graphene sheet across a step-edge on the (111)-oriented STO substrate. In addition a small no-crossing band gap opens in the linear electronic spectrum of graphene.

Acknowledgements

We thank Agham Posadas and Chungwei Lin for critically reading the manuscript, and Hosung Seo for helpful discussions. Support for this work was provided through Scientific Discovery through Advanced Computing (SciDAC) program funded by U.S. Department of Energy, Office of Science, Advanced Scientific Computing Research and Basic Energy Sciences under award number DESC0008877.

*demkov@physics.utexas.edu

References

[1] A. H. Castro Neto, F. Guinea, N. M. R. Peres, K. S. Novoselov, and A. K. Geim, Rev. Mod. Phys. **81**, 109 (2009).

[2] S. Das Sarma, S. Adam, E. H. Hwang, and E. Rossi, Rev. Mod. Phys. **83**, 407 (2011).
[3] K. S. Novoselov, A. K. Geim, S. V. Morozov, D. Jiang, Y. Zhang, S. V. Dubonos, I. V. Grigorieva, and A. A. Firsov, Science **306**, 666 (2004).
[4] K. S. Novoselov, A. K. Geim, S. V. Morozov, D. Jiang, M. I. Katsnelson, I. V. Grigorieva, S. V. Dubonos, and A. A. Firsov, Nature (London) **438**, 197 (2005).
[5] A. Lherbier, X. Blase, Y. M. Niquet, F. Triozon, and S. Roche, Phys. Rev. Lett. **101**, 036808 (2008).
[6] L. S. Panchakarla, K. S. Subrahmanyam, S. K. Saha, A. Govindaraj, H. R. Krishnamurthy, U. V. Waghmare, and C. N. R. Rao, Adv. Mater. **21**, 4726 (2009).
[7] Z. Jin, J. Yao, C. Kittrell, and J. M. Tour, ACS Nano **5**, 4112 (2011).
[8] D. Usachov, O. Vilkov, A. Grüneis, D. Haberer, A. Fedorov, V. K. Adamchuk, A. B. Preobrajenski, P. Dudin, A. Barinov, M. Oehzelt, C. Laubschat, and D. V. Vyalikh, Nano Lett. **11**, 5401 (2011).
[9] L. Zhao, R. He, K. T. Rim, T. Schiros, K. S. Kim, H. Zhou, C. Gutiérrez, S. P. Chockalingam, C. J. Arguello, L. Pálová, D. Nordlund, M. S. Hybertsen, D. R. Reichman, T. F. Heinz, P. Kim, A. Pinczuk, G. W. Flynn, and A. N. Pasupathy, Science **333**, 999 (2011).
[10] S. Kamoi, J. G. Kim, N. Hasuike, K. Kisoda, and H. Harima, Jpn. J. Appl. Phys. **54**, 115101 (2015).
[11] M. C. Lemme, T. J. Echtermeyer, M. Baus, and H. Kurz, IEEE Electron Device Lett. **28**, 282 (2007).
[12] I. Meric, M. Y. Han, A. F. Young, B. Ozyilmaz, P. Kim, and K. L. Shepard, Nature Nanotech. **3**, 654 (2008).
[13] D. B. Farmer, H.-Y. Chiu, Y.-M. Lin, K. A. Jenkins, F. Xia, and P. Avouris, Nano Lett. **9**, 4474 (2009).
[14] J. Kedzierski, H. Pei-Lan, A. Reina, J. Kong, P. Healey, P. Wyatt, and C. Keast, IEEE Electron Device Lett. **30**, 745 (2009).
[15] X. Li, W. Cai, J. An, S. Kim, J. Nah, D. Yang, R. Piner, A. Velamakanni, I. Jung, E. Tutuc, S. K. Banerjee, L. Colombo, and R. S. Ruoff, Science **324**, 1312 (2009).
[16] Y.-M. Lin, K. A. Jenkins, A. Valdes-Garcia, J. P. Small, D. B. Farmer, and P. Avouris, Nano Lett. **9**, 422 (2009).
[17] J. S. Moon, D. Curtis, M. Hu, D. Wong, C. McGuire, P. M. Campbell, G. Jernigan, J. L. Tedesco, B. VanMil, R. Myers-Ward, C. Eddy, Jr., and D. K. Gaskill, IEEE Electron Device Lett. **30**, 650 (2009).
[18] L. Liao, J. Bai, Y. Qu, Y. C. Lin, Y. Li, Y. Huang, and X. Duan, Proc. Nat. Acad. Sci. USA **107**, 6711 (2010).
[19] Y.-M. Lin, C. Dimitrakopoulos, K. A. Jenkins, D. B. Farmer, H.-Y. Chiu, A. Grill, and P. Avouris, Science **327**, 662 (2010).
[20] M. H. Rümmeli, A. Bachmatiuk, A. Scott, F. Börrnert, J. H. Warner, V. Hoffman, J.-H. Lin, G. Cuniberti, and B. Büchner, ACS Nano **4**, 4206 (2010).

[21] J. Chen, Y. Wen, Y. Guo, B. Wu, L. Huang, Y. Xue, D. Geng, D. Wang, G. Yu, and Y. Liu, J. Am. Chem. Soc. **133**, 17548 (2011).
[22] M. A. Fanton, J. A. Robinson, C. Puls, Y. Liu, M. J. Hollander, B. E. Weiland, M. LaBella, K. Trumbull, R. Kasarda, C. Howsare, Joseph Stitt, and D. W. Snyder, ACS Nano **5**, 8062 (2011).
[23] H. Bi, S. Sun, F. Huang, X. Xie, and M. Jiang, J. Mater. Chem. **22**, 411 (2012).
[24] H. Medina, Y.-C. Lin, C. Jin, C.-C. Lu, C.-H. Yeh, K.-P. Huang, K. Suenaga, J. Robertson, and P.-W. Chiu, Adv. Funct. Mater. **22**, 2123 (2012).
[25] H. J. Song, M. Son, C. Park, H. Lim, M. P. Levendorf, A. W. Tsen, J. Park, and H. C. Choi, Nanoscale **4**, 3050 (2012).
[26] J. Chen, Y. Guo, Y. Wen, L. Huang, Y. Xue, D. Geng, B. Wu, B. Luo, G. Yu, and Y. Liu, Adv. Mater. **25**, 992 (2013).
[27] J. Hwang, M. Kim, D. Campbell, H. A. Alsalman, J. Y. Kwak, S. Shivaraman, A. R. Woll, A. K. Singh, R. G. Hennig, S. Gorantla, M. H. Rümmeli, and M. G. Spencer, ACS Nano **7**, 385 (2013).
[28] S. Bae, H. Kim, Y. Lee, X. Xu, J. Park, Y. Zheng, J. Balakrishnan, T. Lei, H. R. Kim, Y. I. Song, Y.-J. Kim, K. S. Kim, B. Özyilmaz, J.-H. Ahn, B. H. Hong, and S. Iijima, Nature Nanotech **5**, 574 (2010).
[29] Y. Zheng, G.-X. Ni, C.-T. Toh, M.-G. Zeng, S.-T. Chen, K. Yao, and B. O□zyilmaz, Appl. Phys. Lett. **94**, 163505 (2009).
[30] Y. Zheng, G. X. Ni, C. T. Toh, C. Y. Tan, K. Yao, and B. Ozyilmaz, Phys. Rev. Lett. **105**, 166602 (2010).
[31] Y. Zheng, G.-X. Ni, S. Bae, C.-X. Cong, O. Kahya, C.-T. Toh, H. R. Kim, D. Im, T. Yu, J. H. Ahn, B. H. Hong, and B. O□zyilmaz, Europhys. Lett. **93**, 17002 (2011).
[32] X. Hong, A. Posadas, K. Zou, C. H. Ahn, and J. Zhu, Phys. Rev. Lett. **102**, 136808 (2009).
[33] D. Jin, A. Kumar, K. Hung Fung, J. Xu, and N. X. Fang, Appl. Phys. Lett. **102**, 201118 (2013).
[34] P. K. Gogoi, P. E. Trevisanutto, M. Yang, I. Santoso, T. C. Asmara, A. Terentjevs, F. D. Sala, M. B. H. Breese, T. Venkatesan, Y. P. Feng, K. P. Loh, A. H. Castro Neto, and A. Rusydi, Phys. Rev. B **91**, 035424 (2015).
[35] P. A. Khomyakov, G. Giovannetti, P. C. Rusu, G. Brocks, J. van den Brink, and P. J. Kelly, Phys. Rev. B **91**, 195425 (2009).
[36] A. Ohtomo and H. Y. Hwang, Nature (London) **427**, 423 (2004).
[37] W. A. Harrison, E. A. Kraut, J. R. Waldrop, and R. W. Grant, Phys. Rev. B **18**, 4402 (1978).
[38] H. Y. Hwang, Science **313**, 1895 (2006).
[39] J. Lee and A. A. Demkov, Phys. Rev. B **78**, 193104 (2008).
[40] H. Seo and A. A. Demkov, Phys. Rev. B **84**, 045440 (2011).
[41] B. Huang, H. J. Xiang, and S.-H. Wei, Phys. Rev. B **83**, 161405(R) (2011).

[42] Z. Chen, I. Santoso, R. Wang, L. F. Xie, H. Y. Mao, H. Huang, Y. Z. Wang, X. Y. Gao, Z. K. Chen, D. Ma, A. T. S. Wee, and W. Chen, Appl. Phys. Lett. **96**, 213104 (2010).
[43] Y. S. Shin, J. Y. Son, M. H. Jo, Y. H. Shin, and H. M. Jang, J. Am. Chem. Soc. **133**, 5623 (2011).
[44] G. Kresse and J. Furthmüller, Phys. Rev. B **54**, 11169 (1996).
[45] P. E. Blöchl, Phys. Rev. B **50**, 17953 (1994).
[46] S. Grimme, J. Comput. Chem. **27**, 1787 (2006).
[47] P. E. Trevisanutto, C. Giorgetti, L. Reining, M. Ladisa, and V. Olevano, Phys. Rev. Lett. **101**, 226405 (2008).
[48] C. G. Van de Walle, Phys. Rev. B **39**, 1871 (1989).
[49] J. Robertson and C. W. Chen, Appl. Phys. Lett. **74**, 1168 (1999).
[50] A. A. Demkov, L. R. C. Fonseca, E. Verret, J. Tomfohr, and O. F. Sankey, Phys. Rev. B **71** (2005).
[51] W. Schottky, Z. Phys. **118**, 539 (1942).
[52] J. Bardeen, Phys. Rev. **71**, 717 (1947).
[53] K. van Benthem, C. Elsa□sser, and R. H. French, J. Appl. Phys. **90**, 6156 (2001).
[54] A. Ohtomo and H. Y. Hwang, Appl. Phys. Lett. **84**, 1716 (2004).
[55] Y.-J. Yu, Y. Zhao, S. Ryu, L. E. Brus, K. S. Kim, and P. Kim, Nano Lett. **9**, 3430 (2009).
[56] E. Mikheev, B. D. Hoskins, D. B. Strukov, and S. Stemmer, Nature Commun. **5**, 3990 (2014).
[57] C. Lin, C. Mitra, and A. A. Demkov, Phys. Rev. B **86** (2012).
[58] C. Mitra, C. Lin, J. Robertson, and A. A. Demkov, Phys. Rev. B **86** (2012).
[59] C. Lin and A. A. Demkov, Phys. Rev. Lett. **111**, 217601 (2013).
[60] F. El-Mellouhi, E. N. Brothers, M. J. Lucero, and G. E. Scuseria, J. Phys.: Condens. Matter **25**, 135501 (2013).
[61] D. M. Bylander and L. Kleinman, Phys. Rev. B **36**, 3229 (1987).
[62] P. R. Wallace, Phys. Rev. **71**, 622 (1947).

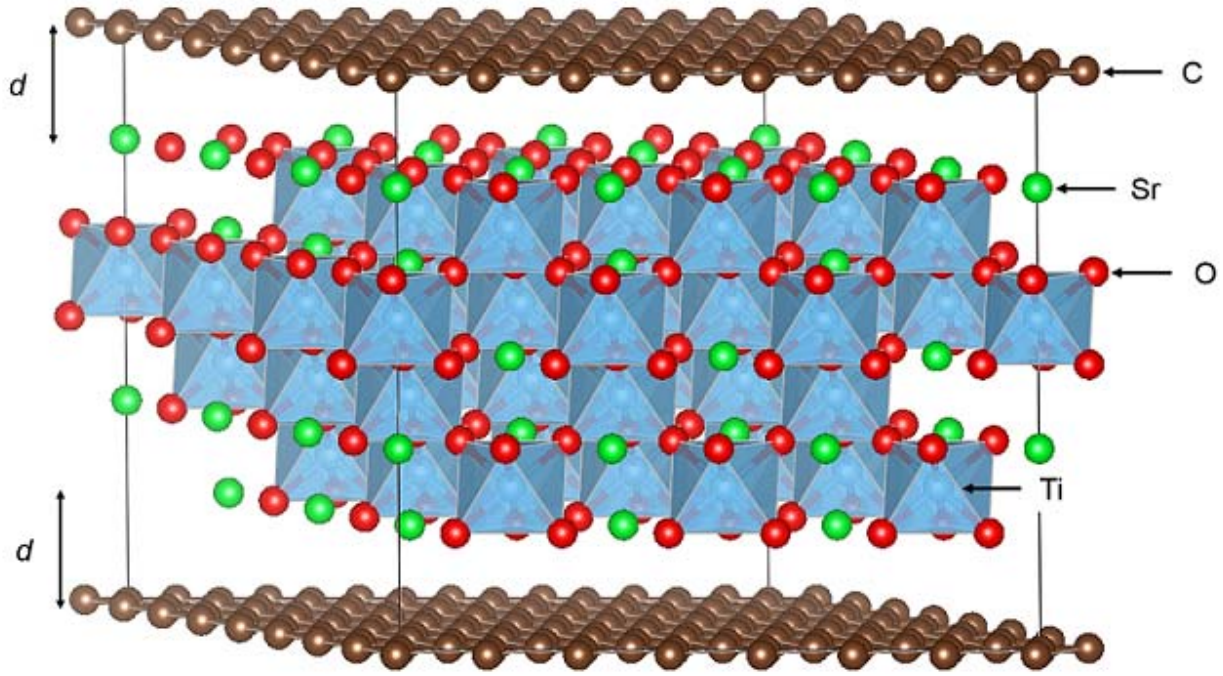

Figure 1 A simulation cell used to model a single layer graphene on STO (111).

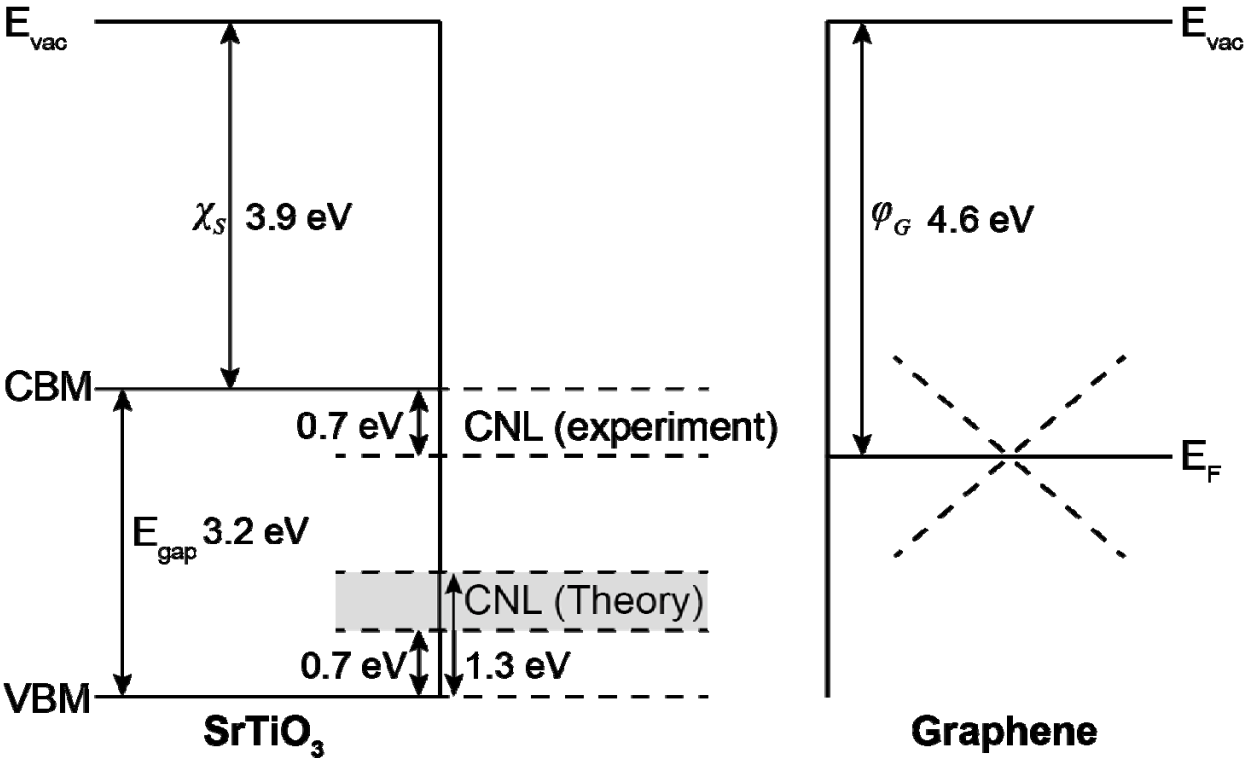

Figure 2. Schematic of the energy bands of STO and graphene (essentially the alignment in the Schottky limit). The experimental values for the graphene work function and STO electron affinity and band gap are shown. Two estimates, using experimental and theoretical values of STO CNL are also indicated. The CNL estimated using the complex band structure is calculated to be 0.7 – 1.3 eV above the VBM [50]. The conduction band offset within the Schottky limit is expected to be 0.7 eV.

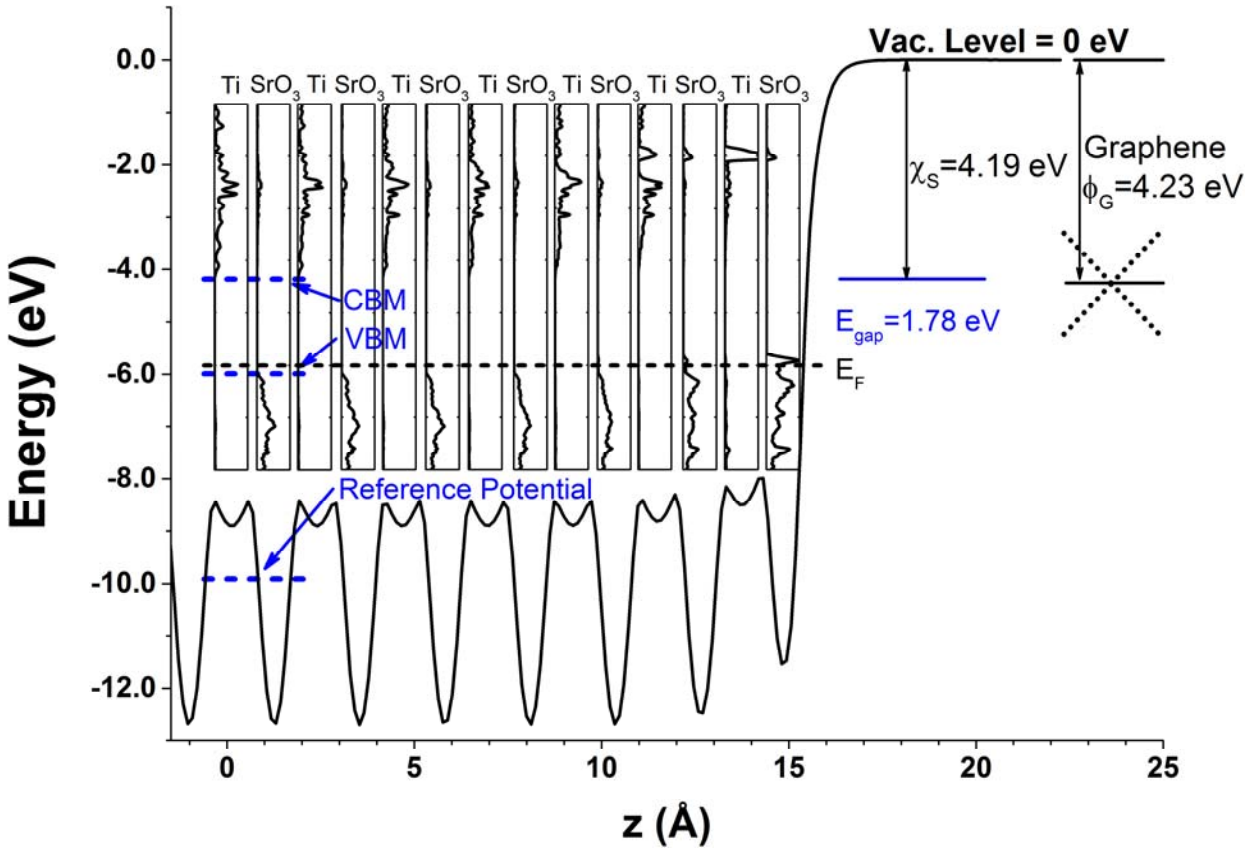

Figure 3. Plane-averaged electrostatic potential as a function of distance (z) normal to the (111) surface and layer projected density of states (pDOS) for a half of asymmetric, twenty-seven-layer-thick, (111)-oriented STO slab. The vacuum level is set to zero. Black dashed line shows the Fermi level. Blue dashed lines indicate the conduction band minimum, the valence band maximum, and the reference average potential. In the pDOS, the vertical axis represents energy and horizontal axis represents DOS in arbitrary units. The GGA-estimated electron affinity of STO (χ_S) and work function of graphene (ϕ_G) are shown in the right side of figure.

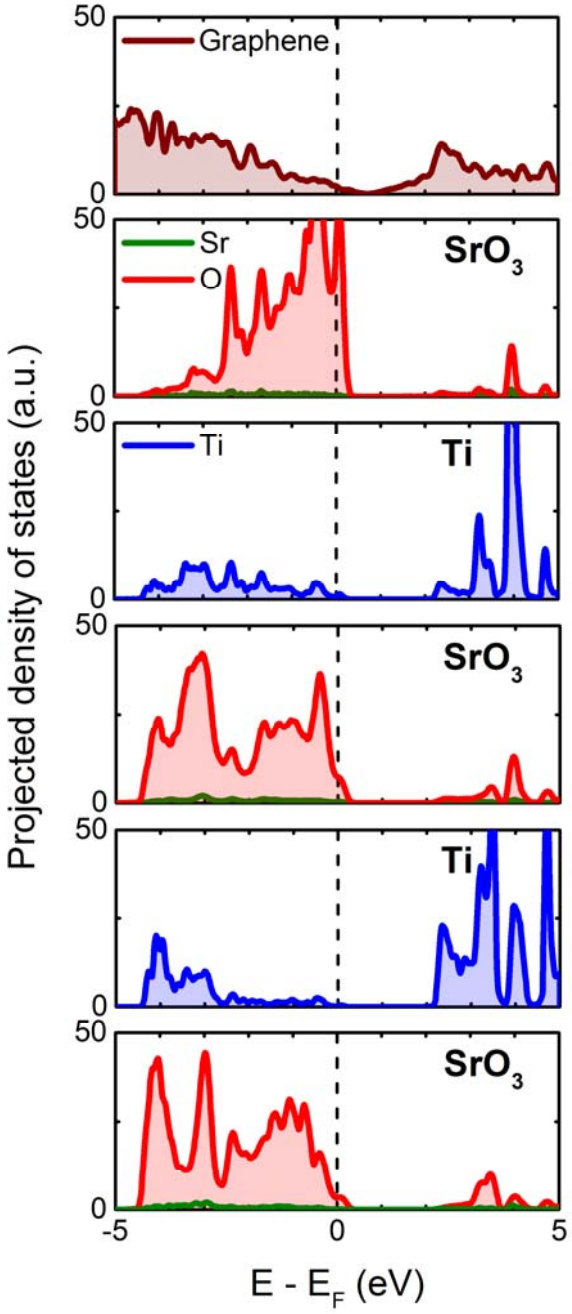

Figure 4. A layer-by-layer atom-projected DOS of the graphene on STO (111) (color on line). The dashed line represents the Fermi level. The brown, green, red, and blue colors represent C, Sr, O, and Ti atoms, respectively. We only plot data for the upper part of the slab because our cell is symmetric with respect to the central layer (bottom SrO_3 panel in the figure).

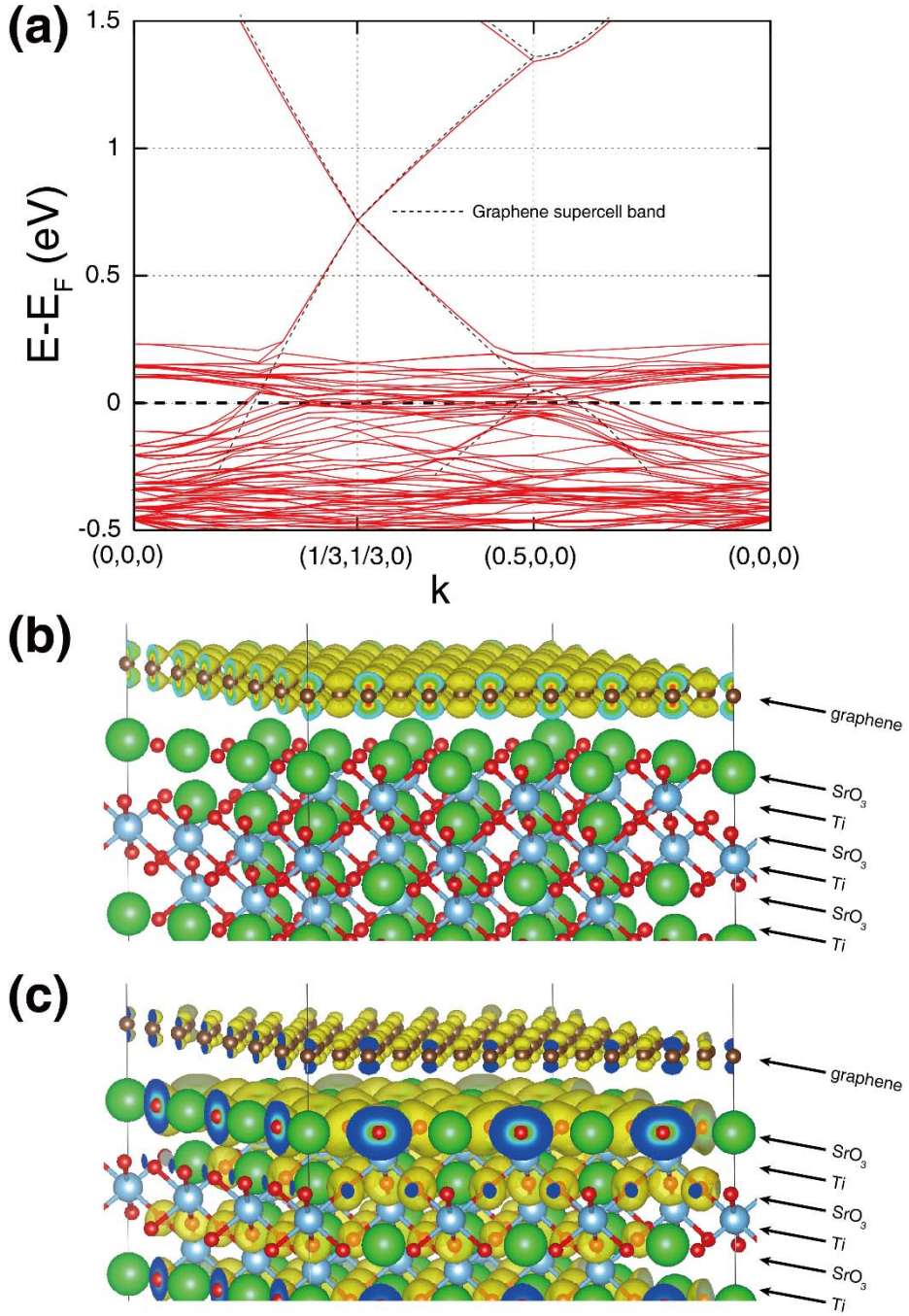

Figure 5. (a) Band structure of graphene on STO (111). A dashed line represents the Fermi level which is set to zero. Probability distribution calculated within the energy window (± 0.03 eV) corresponding to the band crossing point (b) and charge density corresponding to the Fermi level (c). It shows the charge density of graphene sheet and the surface of STO (111). Saturation level is set to (b) 0.0001 e/Å^3 and (c) 0.0003 e/Å^3. The brown, green, red, and cyan balls represents C, Sr, O, and Ti atoms respectively.

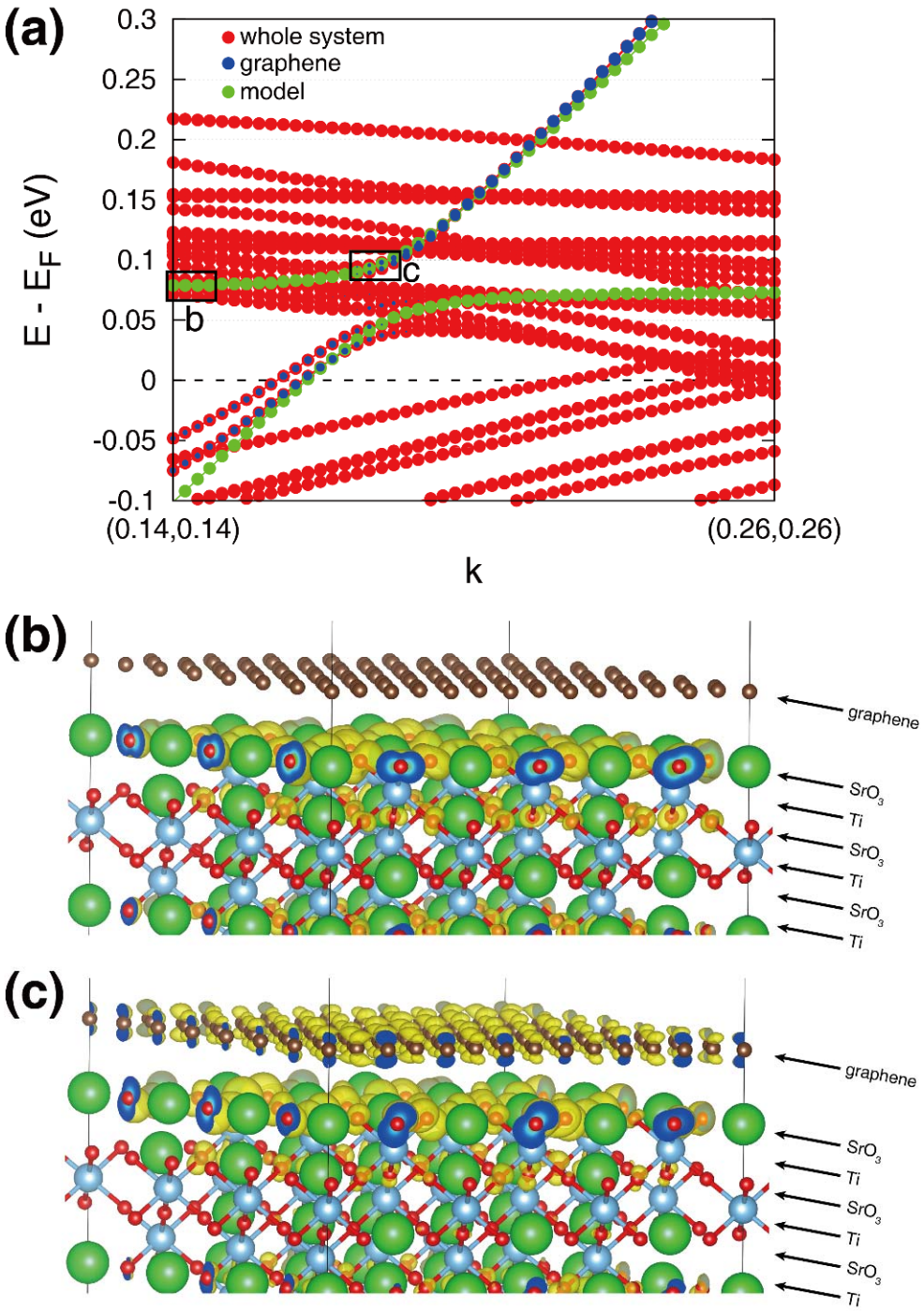

Figure 6. (a) A zoomed-in band structure of graphene on STO (111). The Fermi energy is set to zero. Blue dots represent the graphene contribution to the electronic bands. The size of the blue dot indicates the degree of contribution. Green dots represent the eigenvalues from the two-band model described in the text. The probability distribution corresponding to the STO surface state (b) and the no-crossing region (c). Rectangles in (a) indicate the range of each calculation for (b) and (c). Saturation level is set to (b) 0.001 e/Å^3 and (c) 0.0005 e/Å^3. The brown, green, red, and cyan balls represents C, Sr, O, and Ti atoms respectively.